Dam breaking by wave-induced erosional incision

Dam breaking by wave-induced erosional incision

N. J. Balmforth,[1] J. von Hardenberg,[2] A. Provenzale,[2] and R. Zammett[3]

Received 23 January 2007; revised 25 October 2007; accepted 28 November 2007; published 18 March 2008.

[1] We present an experimental and theoretical study of whether a large displacement wave can lead to catastrophic erosional incision of a moraine damming a glacial lake. The laboratory experiments consist of reservoirs held by barriers of granular materials in a glass tank; the theoretical model combines the Saint-Venant equations of hydraulic engineering with an empirical prescription for erosion. The results of both the laboratory experiments and the numerical simulations indicate that a single wave is generally unable to break the dam, but a sufficiently large disturbance in an almost-filled reservoir creates a seiche that can repeatedly overtop the dam. In such a case, the combined effect of the multiple erosion events ultimately breaks the dam.

Citation: Balmforth, N. J., J. von Hardenberg, A. Provenzale, and R. Zammett (2008), Dam breaking by wave-induced erosional incision, *J. Geophys. Res.*, *113*, F01020, doi:10.1029/2007JF000756.

1. Introduction

[2] As a result of recent climate warming, many moraine-dammed lakes have been left behind by retreating glaciers in mountainous regions worldwide. These lakes are typically hundreds of meters wide and tens of meters deep, and pose a significant flood hazard if the dam can be breached relatively swiftly. Geological observations suggest that several catastrophic dam failures have indeed occurred in recent years and released destructive flood waves [*Clague and Evans*, 2000]. For example, the moraine that dammed Queen Bess Lake (British Columbia) was breached in a sudden event in 1997 that lasted a few hours and emptied six million cubic meters of water [*Kershaw et al.*, 2005]. The current article focuses on a particular mechanism by which dam breaks of this kind could have occurred.

[3] Natural dams are known to fail in a variety of ways [e.g., *Costa and Schuster*, 1988] and the style of the dam break depends on the geological setting. The breach of earthen dams, of either natural or man-made origin, is often associated with severe flooding events, and it has been subject to intense investigation. Most studies focused on the breach of constructed earthen dams by overfilling of the dammed reservoir [e.g., *McDonald and Langridge-Monopolis*, 1984; *Wurbs*, 1987; *Singh and Scarlators*, 1988; *Froehlich*, 1995; *Singh*, 1996; *Walder and O'Connor*, 1997; *Tingsanchali and Chinnarasri*, 2001; *Coleman et al.*, 2002; *Cao et al.*, 2004; *Wang and Bowles*, 2006a, 2006b]. Under such conditions, the constant water flow atop the dam can lead to rapid erosion and to the formation of an incipient outflow channel. Water flow through this conduit leads to further erosion that deepens it, elevating the rate of erosion and deepening the channel still further. A runaway ensues that only declines when the lake level falls low enough to reduce the water flux through the incised channel and turn off erosion.

[4] As evidenced by several sites where incised outflow channels are found on broken moraine dams [see *Clague and Evans*, 2000], runaway erosional incision can also breach moraines damming glacial lakes. In a few of these examples, the incipient channel that triggers the runaway is thought to have been created by the gradual overfilling of the lake (because of extreme climate conditions or intense glacier melting). However, several other dam-break events appear to have been triggered by a different mechanism, specifically overtopping by a large displacement wave. Large displacement waves can be generated by avalanches or rockfalls in the mountainous environments of glaciers, or by icefalls from a retreating glacial toe. The evidence at Queen Bess lake points to an ice fall as the trigger of the dam break [*Kershaw et al.*, 2005], while a landslide at Laguna Safuna Alta (Peru) apparently generated a displacement wave over one hundred meters high which significantly eroded the moraine dam, but left it intact [*Hubbard et al.*, 2005].

[5] Despite the intuitive simplicity of the idea behind catastrophic erosional incision by a large wave, there are a number of possible difficulties with this explanation. Many moraine-dammed lakes are stable structures since they have survived for centuries, and there are examples of waves that did not breach the dam, as in the case of Laguna Safuna Alta. Thus it is not that easy to break a moraine. Indeed, overtopping waves may carry enough water over the dam to drain the lake sufficiently to avoid any subsequent outflow. Finally, erosion is normally a slow process on the hydrodynamic timescale that characterizes the passage of a displacement wave; it is not clear whether sufficient erosion could take place during the relatively fast traversal of the dam.

[6] To explore some of these issues, we devised a laboratory experiment to assess whether a wave could trigger runaway erosional incision, finding a positive answer to this question. A detailed description of the laboratory experiments is given in section 2. Encouraged by the

[1]Departments of Earth and Ocean Science and Mathematics, University of British Columbia, Vancouver, British Columbia, Canada.
[2]Institute of Atmospheric Sciences and Climate, CNR, Torino, Italy.
[3]Department of Mathematics, University of Oxford, Oxford, UK.

0148-0227/08/2007JF000756

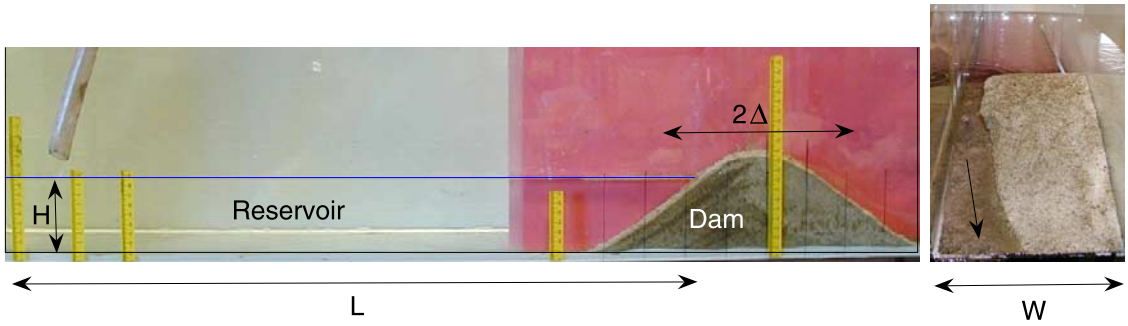

Figure 1. Illustration of the experimental setup. The left-hand picture shows the view from the side, through the glass wall of the tank. The right-hand panel shows a view up the channel from the open end of the tank; here the dam has already broken due to the formation of an outflow channel adjacent to the left wall. H is the water depth in the undisturbed, moraine dammed lake; L is the horizontal size of the reservoir in the cross-moraine direction (x); 2Δ is the full width of the dam at half maximum height; W is the lateral width of the channel in the along-moraine direction (y). The black arrow indicates the flow direction.

experimental results, we advanced further and built a theoretical model similar to those used in hydraulic engineering. The hydraulic model couples a shallow-water-type description of the fluid (actually the Saint-Venant equations) with an empirical erosion law, and it is discussed in section 3. In section 4 we draw some general conclusions and make some remarks about the relevance of our results for geological applications. In the Appendix A we describe some additional features of the theoretical model which bear upon channelization instability and bed form dynamics as often observed prior to or during dam-break events.

2. Exploratory Experiments

[7] Our experimental setup is illustrated in Figure 1. A dam of granular material was built inside a glass tank, and the area to one side was filled with water to create a reservoir. The dam is made of a mixture of roughly equal amounts of fine sand (mean particle size 0.25 mm) and coarse grit (rough, angular particles with mean diameters of about a millimeter). The density and porosity of this material were estimated to be about 2.4 g/cm^3 and 0.3, respectively, and its angle of repose (when dry) was between 33° and 38.5°. The tank measured 30 cm wide and 125 cm long; in some of the experiments, we slightly tilted the tank to provide an overall bottom slope of a few degrees with respect to the horizontal. The dam was built up to a height of about 10–15 cm with a width of 30–40 cm. In different experiments the dam was positioned leaving a reservoir 40 cm or 100 cm long on one side. We then waited a short while in order to allow the water to soak into the dam and judge its stability against seepage. When we were convinced that the dam held against the water pressure, we then tried to break the dam by launching waves toward it. The waves were produced by moving a paddle at the back end of the reservoir; the wave amplitude was estimated from videocam recordings.

[8] After some practice (specifically, varying the initial wave amplitude and the material from which the dam was built), we were able to initiate a catastrophic erosional incision using overtopping waves. A sequence of photographs showing a ''successful'' experiment is shown in Figure 2. The sequence lasts 42 s, and begins as the launched wave breaks over the crest of the dam, and ends when the dam failure is in full progress (the flood ends about 30 s later when the reservoir has largely emptied).

[9] The overtopping wave in the first image of Figure 2 is not particularly deep, primarily because much of the energy of the original disturbance has been reflected back into the reservoir by the dam. Moreover, the erosion generated by the passage of that wave as it washes over the dam is insufficient to cut an incipient channel. The second image shows the dam after the initial wave has passed; some erosion of the downstream face is evident, but there are no incisions on its crest (deposition is also evident near the original foot of the dam). In essence, the wave is too fast to erode a channel, and if all hydrodynamic activity ended at this stage, the dam would not be breached. However, because the dam reflects much of the wave energy back into the lake before the first flooding event, the story continues: the upstream moving disturbance subsequently hits the back wall of the reservoir and is reflected a second time back toward the dam. This generates a second flooding event, with further erosion. Repeated reflections lead to a succession of erosive floods, and although the wave amplitude decreases with each event, the cumulative effect is to eventually incise the channel and breach the dam.

[10] In the experiment shown in Figure 2, over twenty wave reflections occurred before the catastrophic incision ensues. As a result, the reflecting wave in the lake increasingly resembles a seiche-like (normal-mode) motion before breach occurs. In other experiments, as few as five or six wave reflections were sufficient to cut an incipient channel, and the precise number required depended on the initial wave amplitude. Indeed, from the experimental results it rapidly became clear that there was a threshold in the initial wave amplitude below which the dam did not break; as one approached this threshold from above, the number of overspilling seiches needed to breach the dam grew larger.

[11] Figure 3 shows data extracted from an experiment in which about ten seiche oscillations broke the dam. In this case, the outflow channel forms adjacent to one of the glass walls, allowing detailed observations of its bed. Displayed

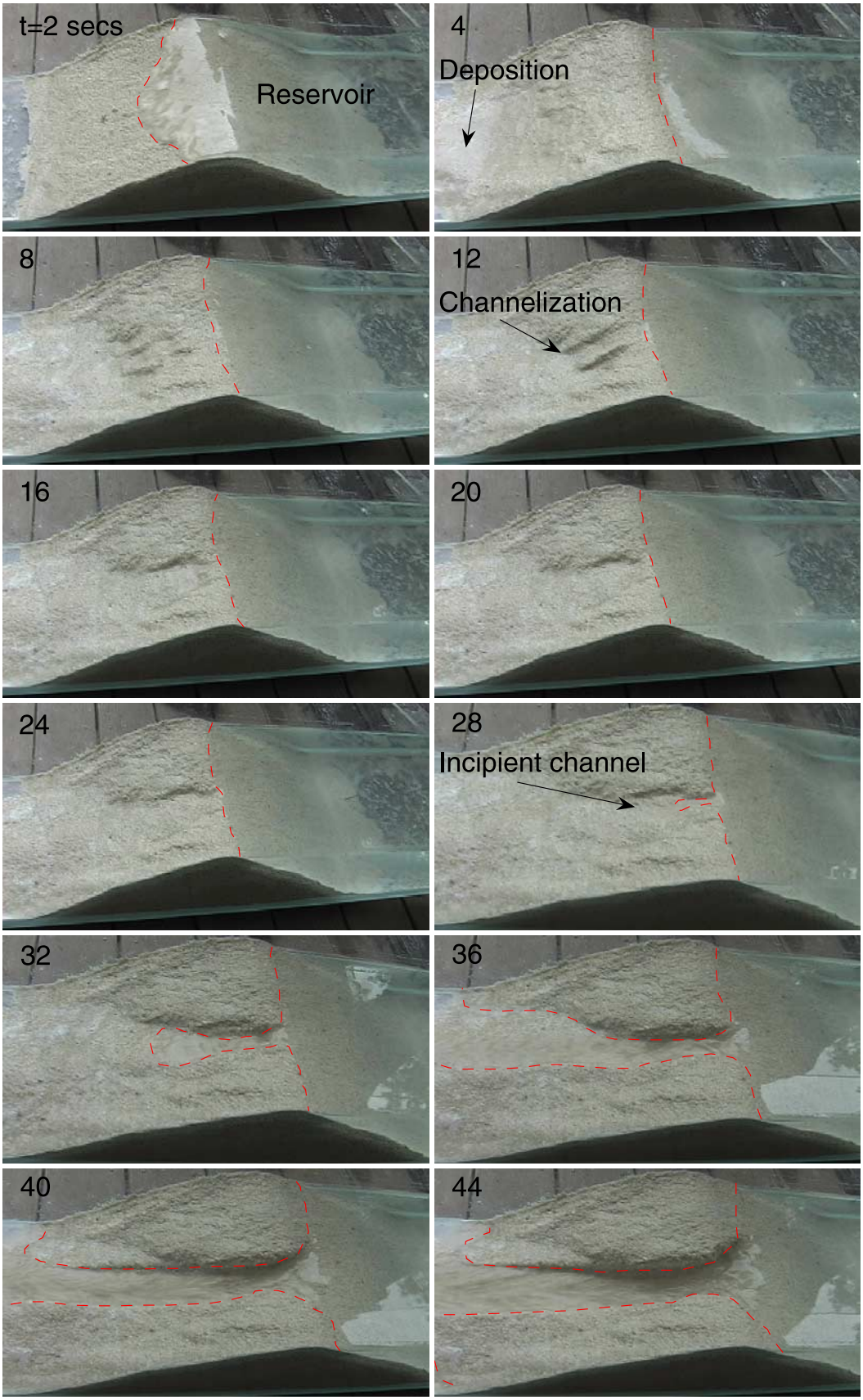

Figure 2. A sequence of photographs showing the catastrophic incision of a dam in the tank initiated by launching a wave over it. The images are 4 s apart.

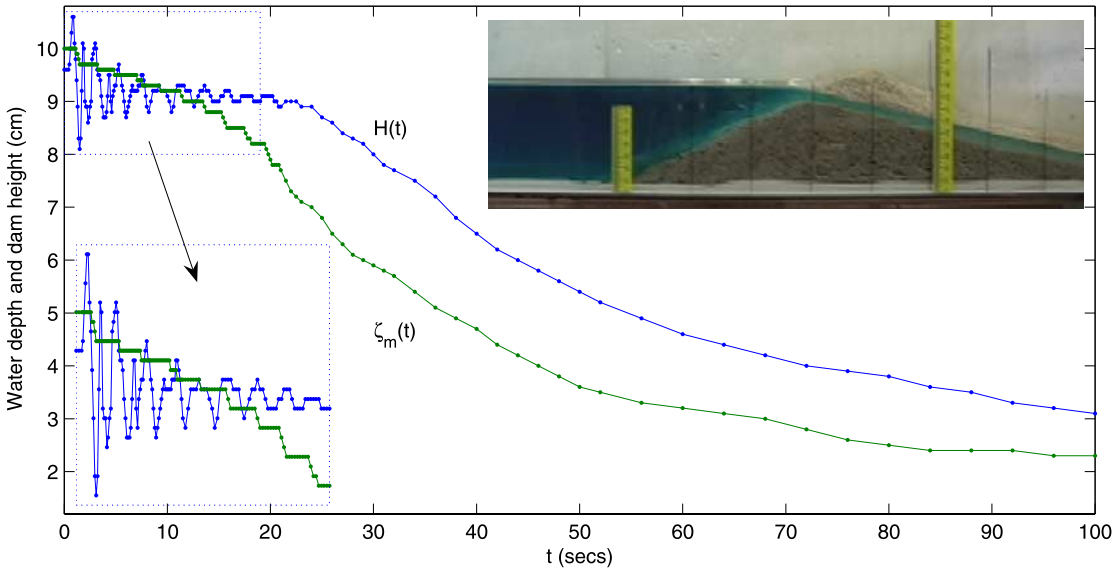

Figure 3. Time series of water depth, $H(t)$, and dam height, $\zeta_m(t)$, extracted from a dam-break experiment. The water depth is measured a short distance upstream of the dam, and the dam maximum, $\zeta_m(t)$, is defined as the highest point on the bed of the outflow channel which forms adjacent to the glass wall of the tank (see the inset photograph; the water has been dyed for visualization). The lower inset shows a magnification of the first period of the evolution, before dam break, to illustrate the seiche-like oscillations.

are measurements of water depth, as recorded just to the left of the dam ($H(t)$), and the dam height, given by the highest point on the bed of the outflow channel ($\zeta_m(t)$). The oscillations in water depth reveal the decaying seiche of the reservoir, and the step-like fall of the dam height reflects the episodic incisions.

[12] The downstream face of the dam in Figure 2 becomes channelized by erosion, and three or four distinct grooves are cut during the initial phases of the dam break. Eventually, one of the grooves deepens more than the others and takes control of the water flow; that incision subsequently widens and deepens further, cutting increasingly far back up the dam. It is this groove that eventually reaches the top of the dam to open a steady outflow, and triggers the catastrophic incision. Channelization patterns on the dam's downstream face were a common type of "bed form" observed in the experiments. Figure 4 shows two more examples. The first example displays a pattern that is fairly periodic; the second shows a top view of the two channels that eventually incise the top of the dam to open up multiple outflows. We comment further on channelization in the next section and in the Appendix A.

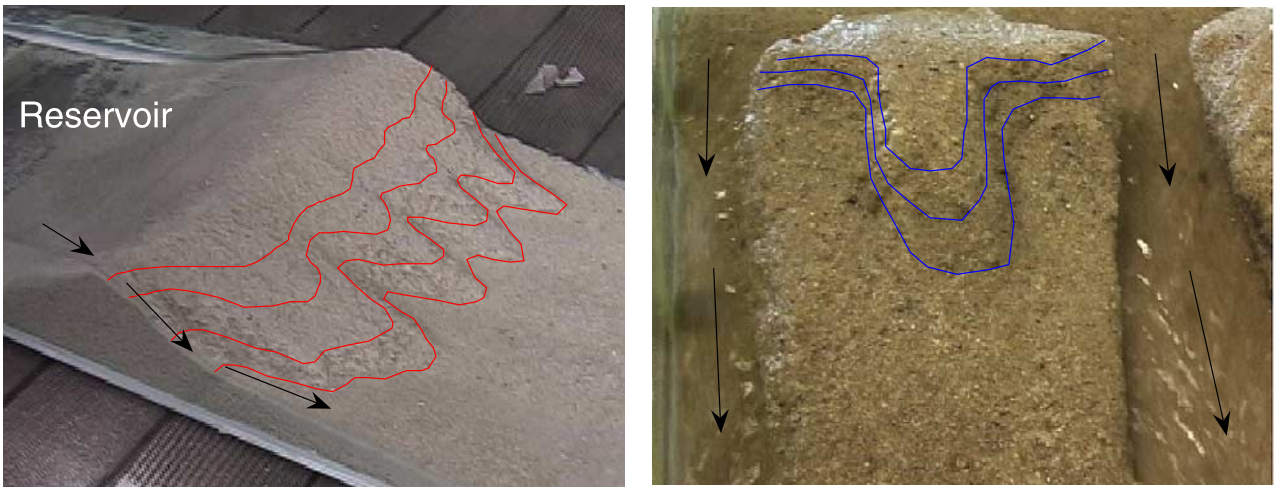

Figure 4. Snapshots of channelization. Five or six grooves have been cut into the downstream face of the dam in the first picture; the nearest groove adjacent to the wall of the tank has deepened most and has created an incipient channel at the top of the dam which is about to trigger catastrophic incision. In the second image, the incision has already taken place. In this case, 4 or 5 grooves were cut, and two of these eventually breached outflow channels in the dam. Black arrows indicate flow direction.

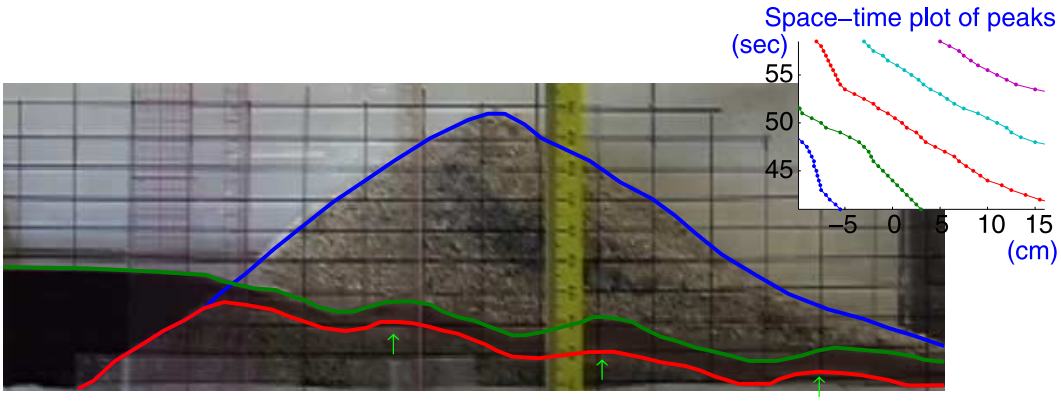

Figure 5. A photograph showing bed forms during a dam breach. Lines highlight the water surface, bed elevation and the relic of the original dam in the background. The inset shows a plot of the spatial positions of the maxima in the bed as functions of time.

[13] Channelization was not the only type of bed form that one could observe. Once the outflow channels were established, upstream-migrating undulations of their beds could also be seen, see Figure 5, but they did not play any key role in the dam-break process. Nevertheless, both the channelization and migrating bed forms reflect the erosional dynamics, and may be thought of as relatives of the instabilities of the flow of a uniform sheet. Indeed, the theoretical model described below captures such instabilities (see the Appendix A).

[14] For completeness, we also considered the case where a constant water flow was forced atop the dam, by filling the reservoir from the bottom of its back side with a flux of about 10^{-3} l/s. In marked contrast to the experiments in which we launched waves at the dam, it was far easier to break this obstruction by overfilling the reservoir. Shortly after water first overtopped the dam, slight variations in dam height selected preferred locations where erosion began, initiating channels that breached the dam in a matter of seconds. Once the runaway incision began, there was little difference in the dam-break dynamics between the overfilling experiments and those with overtopping waves. In other words, once initiated, the runaway is roughly independent of the manner in which it begun.

[15] A final issue concerns the role of the material properties. Fine sand alone could be easily eroded by a passing wave but, once the sand dam became wet, it gradually lost structural strength. Consequently, most often, the downstream face of the dam lost stability, and a catastrophic failure ensued in the form of something like a mudflow. Grit alone held its shape better when wet but it could be eroded less easily by a wave, and water seeped too easily through the dam, draining the reservoir before it could be broken. The sand-grit mixture proved a good compromise: the sand allowing for fast erosion and less seepage, while the grit gave the dam structural strength.

[16] Without recourse to any empirical model of the turbulent erosion process, one is tempted to use dimensional analysis to estimate the effectiveness of erosion. For example, by observing the rate at which the dam height decreases, one can arrive at an "erosion speed" that can be compared to the water flow speed [cf., *Walder and O'Connor*, 1997]. Their ratio yields a dimensionless, characteristic erosion speed which is order 10^{-3} in our experiments. One is further tempted to use this measure in order to scale our experiments up to the geophysical problem. However, a simple estimate of this kind misses key details of the erosion, namely that the erosion rate is a strongly nonlinear function of the flow speed (there is a threshold below which there is no erosion, and above which the rate increases dramatically [cf., *Parker*, 2006]). This leads us to grapple with the empirical erosion model described below. Unfortunately, incorporating the nonlinearity of the erosion rate also demands an inclusion of further parameters, which we were unable to measure in our experiments.

3. A Shallow-Water Model

[17] Motivated by the laboratory experiments, we devised a theoretical model to rationalize the observational results on the dam-break process. In the following, we describe the model and the theoretical insights it can provide.

3.1. Governing Equations

[18] Our theoretical approach to the problem is based on the Saint-Venant equations of hydraulic engineering [e.g., *Balmforth and Provenzale*, 2001]: The flow is assumed to vary only slightly with depth (save for a logarithmic bottom boundary layer) and can be described by the local velocity field, $(u(x, y, t), v(x, y, t))$, and the depth of the water layer, $h(x, y, t)$, which satisfy equations representing conservation of mass and momentum:

$$\frac{\partial h}{\partial t}+\frac{\partial}{\partial x}(hu)+\frac{\partial}{\partial y}(hv)=0, \tag{1}$$

$$\frac{\partial u}{\partial t}+u\frac{\partial u}{\partial x}+v\frac{\partial u}{\partial y}=-g\frac{\partial}{\partial x}(\zeta+h)-C_f\frac{\sqrt{u^2+v^2}}{h}u +\frac{\partial}{\partial x}\left(\nu_e\frac{\partial u}{\partial x}\right)+\frac{\partial}{\partial y}\left(\nu_e\frac{\partial u}{\partial y}\right), \tag{2}$$

$$\frac{\partial v}{\partial t}+u\frac{\partial v}{\partial x}+v\frac{\partial v}{\partial y}=-g\frac{\partial}{\partial y}(\zeta+h)-C_f\frac{\sqrt{u^2+v^2}}{h}v +\frac{\partial}{\partial x}\left(\nu_e\frac{\partial v}{\partial x}\right)+\frac{\partial}{\partial y}\left(\nu_e\frac{\partial v}{\partial y}\right), \tag{3}$$

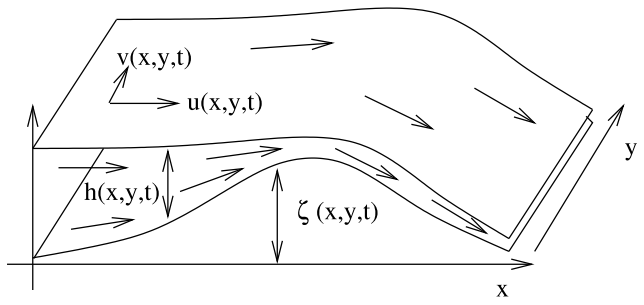

Figure 6. Sketch of the geometry in the theoretical model.

where the surface $z = \zeta(x, y, t)$ represents the underlying bed (see Figure 6), C_f is a friction coefficient that depends on the roughness of the surface over which the fluid flows and measures the stress exerted on the fluid by the bed, and ν_e is a turbulent viscosity. Models of eddy viscosity often prescribe that quantity as a function of flow speed and depth; here we keep the problem as simple as possible and merely take ν_e to be constant. In most of the numerical experiments we have ignored any volume and momentum source terms in the fluid equations, thereby assuming that the suspended sediment does not feed back on the flow dynamics (*Cao et al.* [2004] assess the potential importance of such terms in related dam-break problems). We return to this point at the end of this section.

[19] The bed over which fluid flows is erodible and we require a model for how material is lifted off this surface and transported by the fluid. We borrow heavily from the work of Parker and collaborators [*Parker*, 2006; *Parker and Izumi*, 2000], who deal with different erosional problems [see also *Cao et al.*, 2004]. We assume that the bed is eroded by the overlying fluid with a rate that depends purely on the stress exerted by the fluid on the bed, which is proportional to $u^2 + v^2$. The eroded material is then suspended in the fluid for a time, where it is advected and mixed by turbulence. However, the suspended material also sediments under gravity and falls back on the bed. To model in a crude fashion this dynamics, we use the Exner equation for the surface of the bed,

$$\frac{\partial \zeta}{\partial t} = w_s \frac{C}{h} - w_e E\left(u^2 + v^2\right), \tag{4}$$

in combination with a transport law for the suspended load,

$$\frac{\partial C}{\partial t} + \frac{\partial}{\partial x}(uC) + \frac{\partial}{\partial y}(vC) = \kappa_e\left(\frac{\partial^2 C}{\partial x^2} + \frac{\partial^2 C}{\partial y^2}\right) + w_e E\left(u^2 + v^2\right) - w_s \frac{C}{h}, \tag{5}$$

where w_e parameterizes the speed of erosion, w_s is the sedimentation speed, $C(x, y, t)$ denotes the depth-integrated concentration of the suspended load, $E(u^2 + v^2)$ is a suitable dimensionless function modeling the precise dependence of erosion on stress, and κ_e is a turbulent diffusivity (again assumed constant for simplicity). We take

$$E\left(u^2 + v^2\right) = \begin{cases} 0 & u^2 + v^2 < U_{th}^2, \\ \left[(u^2 + v^2)/U_{th}^2 - 1\right]^\alpha & u^2 + v^2 \geq U_{th}^2, \end{cases} \tag{6}$$

where U_{th} denotes a threshold speed below which erosion does not take place, and α is a parameter put equal 1.5 in all examples [e.g., *Seminara*, 2001 and cited references therein]. In general, the values of U_{th} and α are empirically determined.

3.2. Dimensionless Form

[20] We remove some of the distracting constants from the equations and formulate the important dimensionless groups as follows. Let

$$(x, y) = \Delta(\tilde{x}, \tilde{y}), \quad t = \frac{\Delta}{\sqrt{gH}}\tilde{t}, \quad L = \Delta\tilde{L}, \quad W = \Delta\tilde{W}, \quad (u, v) = \sqrt{gH}(\tilde{u}, \tilde{v}), \quad (h, \zeta, C) = H\left(\tilde{h}, \tilde{\zeta}, \tilde{C}\right), \tag{7}$$

where H and Δ denote respectively the characteristic reservoir depth (or dam height) and dam width, L is the horizontal size of the reservoir and W is the lateral width of the channel. Thence, on dropping the tilde decoration,

$$h_t + (hu)_x + (hv)_y = 0, \tag{8}$$

$$u_t + uu_x + vu_y = -h_x - \zeta_x - c_f \frac{\sqrt{u^2 + v^2}}{h} u + \nu\left(u_{xx} + u_{yy}\right), \tag{9}$$

$$v_t + uv_x + vv_y = -h_y - \zeta_y - c_f \frac{\sqrt{u^2 + v^2}}{h} v + \nu\left(v_{xx} + v_{yy}\right), \tag{10}$$

$$\zeta_t = \epsilon_s \frac{C}{h} - \epsilon E\left(u^2 + v^2\right), \quad E(u^2 + v^2) = \left[\mathrm{Max}\left(0, u^2 + v^2 - u_{th}^2\right)\right]^\alpha, \tag{11}$$

and

$$C_t + (uC)_x + (vC)_y = \kappa\left(C_{xx} + C_{yy}\right) + \epsilon E\left(u^2 + v^2\right) - \epsilon_s \frac{C}{h}, \tag{12}$$

where

$$u_{th} = \frac{U_{th}}{\sqrt{gH}}, \quad \epsilon = \frac{\Delta}{H}\frac{w_e}{\sqrt{gH}}\left(\frac{gH}{U_{th}^2}\right)^\alpha, \quad \epsilon_s = \frac{\Delta}{H}\frac{w_s}{\sqrt{gH}}, \quad \nu = \frac{\nu_e}{\Delta\sqrt{gH}}, \quad \kappa = \frac{\kappa_e}{\Delta\sqrt{gH}}, \quad c_f = C_f\frac{\Delta}{H}, \tag{13}$$

and subscripts x, y and t indicate partial derivatives. The quantity u_{th} can be interpreted as the Froude number for erosion initiation, while the other parameters are respectively the normalized erosion and sedimentation velocities, and the normalized fluid viscosity and sediment diffusivity.

[21] To describe the initial shape of the bed, we assume that there is a non-erodible bottom plane, $\zeta_0(x) = -Sx$, where S is an overall slope parameter. Provided S is small, the results are rather insensitive to its precise value and one can also put $S = 0$. On top of this bottom plane, we distribute erodible material such that the overall bed elevation is

$$\zeta(x,y,0) = [1+\rho(x,y)]\exp\left(-\frac{x^2}{2\sigma^2}\right) + \zeta_0(x), \qquad (14)$$

where σ measures the width of the (Gaussian-shaped) dam and $\rho(x, y)$ is a small (amplitude 5%), random (white noise) perturbation.

[22] The domain spans the interval $[-W/2, W/2]$ in the y-direction and $[-L, L]$ in the x-direction, with L taken large enough to ensure a wide reservoir behind the dam, and sufficient space downstream so that the boundary conditions at $x = L$ play no significant role. The boundary conditions are those of impermeability and free-slip on the upstream and sidewalls: $u = v_x = h_x = C_x = 0$ at $x = -L$, and $v = u_y = h_y = C_y = 0$ on $y = \pm W/2$. At the downstream boundary, $x = L$, "open" boundary conditions are used: $u_x = v_x = h_x = C_x = 0$.

[23] Given the bed structure in (14), the equations have a static lake solution, $u = v = 0$ and

$$h_{eq}(x,y) = \begin{cases} h_0 - \zeta(x,y) & \text{if} \quad h_0 > \zeta \text{ and } x < 0, \\ 0 & \text{otherwise.} \end{cases} \qquad (15)$$

The initial perturbation to this equilibrium consists of a sinusoidal wave with amplitude A, so that the initial water elevation becomes

$$h(x,y,0) = \begin{cases} h_{eq}(x,y) + A\sin(2\pi x/L) & \text{if} \quad x < 0, \\ 0 & \text{if} \quad x \geq 0. \end{cases} \qquad (16)$$

[24] Equations (8)–(12) are integrated numerically with a Leapfrog-Adams-Moulton predictor-corrector scheme in time and a second-order-accurate finite difference scheme in space, using an Arakawa "C" staggered grid [*Arakawa and Lamb*, 1977]. A Flux-Corrected Transport scheme [*Boris and Book*, 1976; *Zalesak*, 1979] is used for the positive definite variables h and C. To avoid any problems with divisions by zero, we replaced the bottom friction terms in equations (9) and (10) by the "regularizations", $-c_f\sqrt{(u^2+v^2)/(h^2+10^{-8})}\,(u, v)$.

3.3. Dam Break Simulations

[25] Figure 7 reports a sequence of model solutions in time, starting from the initial conditions described above, with $c_f = 0.02$ and $\epsilon = 0.12$. Part of the initial wave overtops the dam, leading to erosion of the downstream flank. This leads to the creation of channels which can be rationalized as the channelization instability of a uniform flowing sheet (as described in the Appendix A). A secondary wave is reflected back into the reservoir and sets up a seiche of that water body, exactly as in the experiments. The repeated floodings as the seiches overspill the dam's crest further incise the channels on the downstream flank. After six seiches, a channel ultimately opens up on top of the dam, through which the reservoir water begins to flow unabated. At that stage, the rate of erosion increases rapidly and the channel begins its catastrophic deepening. Eventually, the water is completely evacuated from the upstream basin.

[26] Figure 8 displays further details of the modeled incision process: the first panel shows the evolution in time of the bed elevation at a few selected points; the second illustrates the evolution of the average water height in the upstream basin and of the water flux exiting the domain on the right border. The time series of ζ show a number of small plateau (which represent the periods over which the waves bounce back and forth in the reservoir), divided by sharp steps (the erosion events). At about $t = 125$, the runaway incision takes place, leading to the peak discharge.

[27] Repeating the same experiment at different values of c_f and ϵ_s gives qualitatively similar results. However, the values of both the erosion parameter, ϵ, and initial wave amplitude, A, are critical: if either ϵ or A are decreased, the time for the appearance of the incipient channel increases rapidly as more and more reflections are required and the reflected waves lose their strength. Ultimately, an incision is completely suppressed; Table 1 presents a summary of the results. In other words, there is a threshold for dam break in either the initial wave amplitude, or erosion rate. The former result mirrors our experimental findings.

[28] Before closing this section, we stress the fact that the above results have been obtained by ignoring the feedback of the suspended sediment on the fluid dynamics, a fact that in principle could lead to considerable errors in the case of highly unsteady flows with intensive sediment transport and rapid bed changes [e.g., *Zech and Spinewine*, 2002]. To address, at least in a first approximation, this issue, we have modified the continuity equation and included the effect of the suspended sediment [*Cao et al.*, 2004]. The modified model provides qualitatively analogous results, with a slight shift of the threshold for catastrophic dam break to larger erosion rates. For example using the same values for other parameters as in Figure 7, an erosion rate of $\epsilon = 0.12$ was insufficient to trigger a catastrophic erosion; however, once the erosion rate was increased to $\epsilon = 0.16$, the dam was broken after six seiches. This result provides confidence in the findings obtained with the model without sediment feedback.

4. Discussion

[29] In this work we have described a preliminary exploration of breaking a moraine dam by initiating a displacement wave in the glacial lake. Our main conclusion is that it is feasible to reproduce the catastrophic erosional incision scenario both in simple laboratory experiments and a theoretical shallow-water model. We close by discussing a number of important possible implications of our results and indicating where our work could be extended.

[30] Although it was not our main focus, we also performed a number of experiments and computations with the theoretical model designed to break the dam by gradual overfilling of the lake. These additional efforts (which are

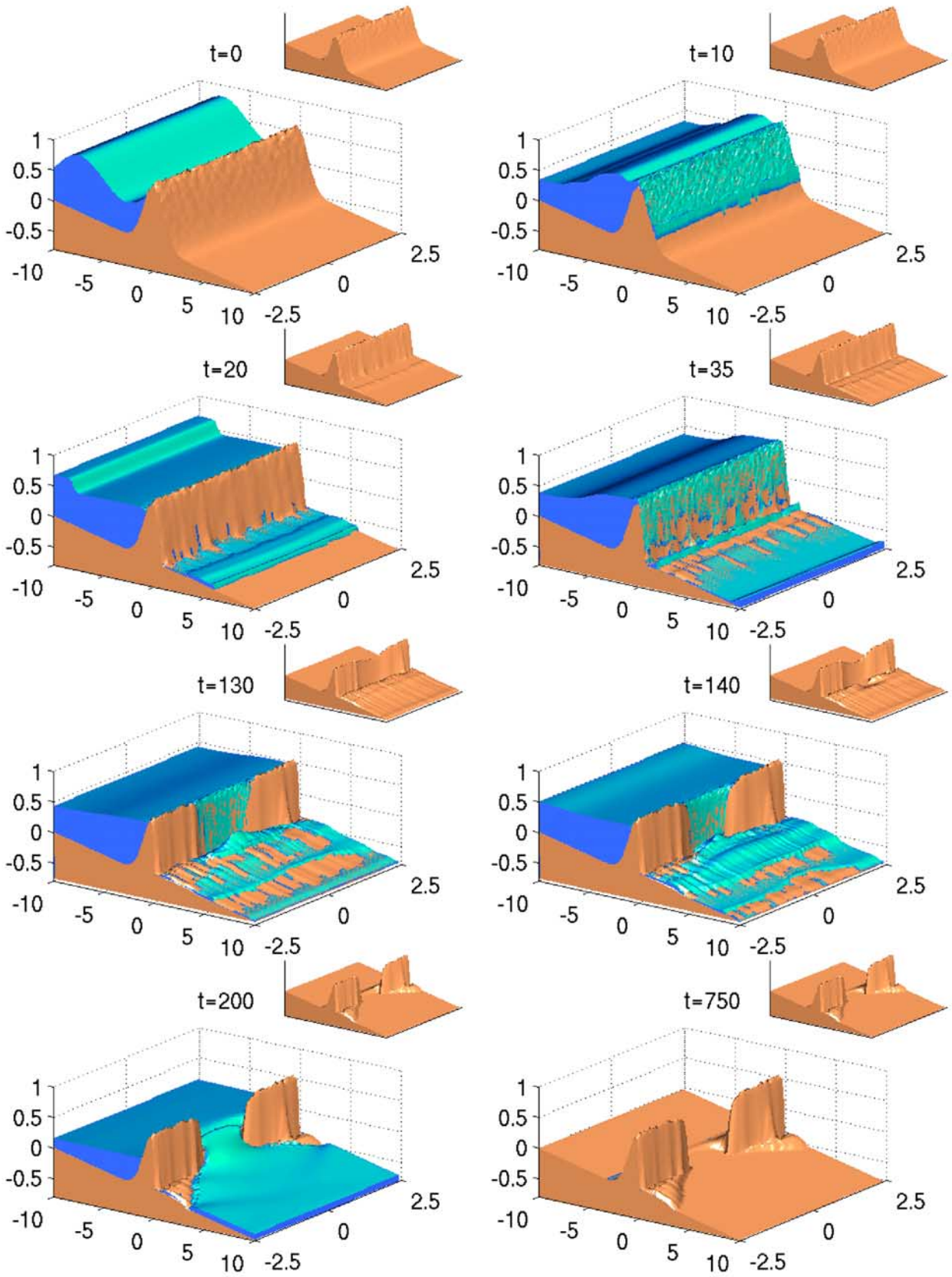

Figure 7. The panels illustrate a numerical experiment of dam-breaking instigated by overtopping waves, showing the evolution of the water surface $h + \zeta$ (blue/dark surface) and bed ζ (brown/light surface; see also the insets). The (nondimensional) parameters used are: $S = 0.04$, $\sigma = 1$, $c_f = 0.02$, $\nu = 0.05$, $\epsilon = 0.12$, $\epsilon_s = 0.002$, $u_{th} = 0.001$, $h_0 = 0.93$, $A = 0.3$, $L = 10$, $W = 5$. The numerical grid resolution was $N_x = 256$, $N_y = 64$.

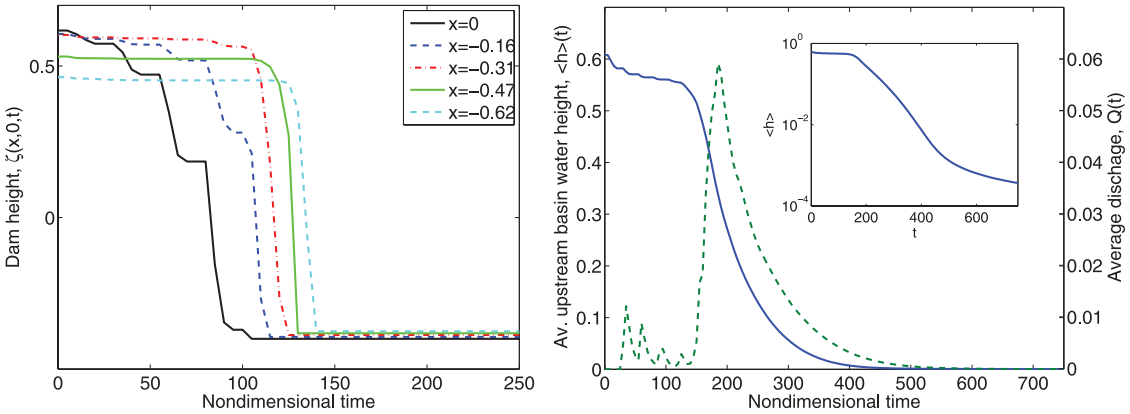

Figure 8. Left panel: Evolution in time of $\zeta(x_i, 0, t)$ at a few selected points x_i; Right panel: Evolution in time of the average water height in the upstream basin (continuous curve), $\langle h\rangle(t) = 1/(LW) \int_{-L}^{0} \int_{-W/2}^{W/2} h(x, y, t)\, dx\, dy$; and the average discharge (dashed curve), $Q(t) = 1/W \int_{-W/2}^{W/2} h(x_1, y, t) u(x_1, y, t)\, dy$, computed at $x_1 = 9.5$. The inset shows the evolution of $\langle h\rangle$ (t) in semilogarithmic coordinates. The simulation is the same as in Figure 7.

similar to previous work on the breaks of earthen dams [e.g., *Coleman et al.*, 2002]) exposed how it was much easier to breach the dam by overfilling the lake than by overtopping it with a displacement wave. This observation contrasts sharply with the summary by *Clague and Evans* [2000], which suggests that overtopping is a more prevalent trigger than overfilling.

[31] For overtopping waves, a crucial detail is the establishment of a seiche in the lake that repeatedly feeds water over the dam; our results indicate that a single wave by itself is not sufficient (unless it breaks the dam through mechanical failure). As a result of these multiple outflows, erosion is able to channelize the downstream face of the dam and cut the incipient channel. Such seiches have also been inferred to occur in the field: for Laguna Safuna Alta, *Hubbard et al.* [2005] concluded that the rockfall generated over ten erosive seiches of the lake. When Queen Bess Lake broke, two distinct surges were recorded in downstream hydrographs, although *Kershaw et al.* [2005] suggested that the main wave and the subsequent incision were responsible. Despite this, an investigation of moraine dam failure in British Columbia suggested (albeit did not definitely prove) that a single wave had created failure in one particular dam [*Blown and Church*, 1985]. In that case, it was suggested that the wave was substantially amplified by a focusing into a restricted opening through the moraine previously occupied by an outflow stream. Careful investigation of wave focusing into existing openings should thus be an important complement to the present analysis.

Table 1. The Number of Seiches Before Dam Break in Simulations With Different A and ε; the Star Indicates no Break[a]

	$\epsilon = 0.08$	$\epsilon = 0.12$	$\epsilon = 0.30$
$A = 0.1$	*	*	*
$A = 0.15$	*	*	5 (397, 0.04)
$A = 0.3$	*	5 (300, 0.05)	2 (113, 0.09)
$A = 0.5$	*	5 (230, 0.1)	3 (101, 0.1)

[a]The remaining parameters are as in Figure 7. In parentheses, the time needed to empty the reservoir (defined as the moment at which the reservoir contains one percent of its original volume) and the peak discharge (the maximum over time of the flux function, $\int u(x, y, t)\, h(x, y, t)\, dy$, at $x = 1$) are noted.

[32] An important facet of the seiching process described here is a threshold, determined by the physical characteristics of the dam material and by the flow dynamics of the overtopping waves, beyond which the system must lie before a catastrophic incision can take place: specifically, there is a competition between erosion, which lowers the dam, and the combined effects of lake drainage and dissipation of the seiche, which decrease the highest water level. The catastrophic incision takes place when the erosion can outpace lake drainage and decay of the seiche. Of course, for the process to work, the lake must be close to full (otherwise the first wave can drain the reservoir sufficiently to prevent a break), and the wave reflected back into the reservoir after the first overtopping must be able to set up a coherent seiche (so the lake geometry cannot be too complicated). Both issues suggest further, interesting geological constraints.

[33] Some extensions of the work presented here are under way. Currently, we are considering a two-dimensional version of the problem, in which we break dams in a narrow tank in order to simplify the dynamics even further and understand more of its details (see *Zammett*, 2006, for a preliminary report). There are also several open issues in the three dimensional situation. For example, the main shortcoming of the theoretical model is the prescription for erosion. The process is itself quite poorly understood, and as we have done here, often mimicked through empirical parameterization. It would be worthwhile to see how dependent theoretical results are on the erosion parameterization. A different, but possibly very important, mechanism is the seepage of water through the dam material and the related structural weakening of the dam itself. Although the laboratory experiments do naturally include this effect, we did not consider it theoretically. The qualitative agreement between simulations and experiments suggests that seepage does not play the leading

role, however, there is clearly a lot more that could be done along these lines.

Appendix A: Channelization Instability of a Flowing Sheet

[34] The equations have a uniform equilibrium solution describing an homogeneous sheet of water flowing down an inclined surface:

$$u = \mathcal{U}, \quad h = 1, \quad v = 0, \quad \zeta = Z = -Sx, \quad C = \mathcal{C} \equiv \frac{\epsilon E(\mathcal{U}^2)}{\epsilon_s}, \tag{A1}$$

where S denotes the inclination, and $c_f \mathcal{U}^2 = S$. Since there is no dam in this problem, we choose Δ such that $C_f \Delta / H = c_f = 1$, to simplify the coming algebra. Note that, if the sedimentation speed $\epsilon_s = 0$ and there is pure erosion, we may ignore C and adopt the uniformly eroding equilibrium, $\zeta = Z = -S\,x - \epsilon\, E(\mathcal{U}^2)\, t$.

[35] It is straightforward to explore the linear stability of the equilibrium solution: We put

$$\begin{aligned} u &= \mathcal{U} + \hat{u} e^{ikx+ily+\lambda t}, \\ v &= \hat{v} e^{ikx+ily+\lambda t}, \\ h &= 1 + \hat{h} e^{ikx+ily+\lambda t}, \\ \zeta &= Z + \hat{\zeta} e^{ikx+ily+\lambda t}, \\ C &= \mathcal{C} + \hat{c} e^{ikx+ily+\lambda t}, \end{aligned} \tag{A2}$$

where (k, l) denote the wave numbers of a wave-like disturbance, and λ is the growth rate, which satisfies the dispersion relation,

$$\begin{aligned} &\left(\lambda + ik\mathcal{U} + 2\mathcal{U} + \nu K^2\right)\left[(\lambda + ik\mathcal{U})\left(\lambda + ik\mathcal{U} + \mathcal{U} + \nu K^2\right) + l^2\right] \\ &\quad + ik\left(\mathcal{U}^2 - ik\right)\left(\lambda + ik\mathcal{U} + \mathcal{U} + \nu K^2\right) \\ &\quad = \frac{\delta(\lambda + ik\mathcal{U})\left[l^2\mathcal{U}^2 + ik(\lambda + ik\mathcal{U})(\lambda + ik\mathcal{U} + \mathcal{U} + \nu K^2)\right]}{\lambda(\lambda + ik\mathcal{U} + \epsilon_s + \kappa K^2)}, \end{aligned} \tag{A3}$$

where $K^2 = k^2 + l^2$ and $\delta = \epsilon \frac{\mathrm{d}E}{\mathrm{d}\mathcal{U}}$.

[36] Our primary interest is in situations with low erosion rates: $\delta \ll 1$. The solutions of the dispersion relation then split into two groups: four roots corresponding to erosionless modes, and a single mode relying on erosion. Of the former, three are hydrodynamic modes and correspond to the linear solutions of the Saint-Venant problem; the fourth is a diffusive mode for sediment concentration. One of the hydrodynamic modes can become unstable when the flow is sufficiently fast. The instability corresponds to the roll waves of *Jeffreys* [1925], which are unstable when $\mathcal{U} > 2$ (equivalently, when the Froude number exceeds 2).

[37] The erosional mode has a growth rate of order δ, which is given approximately by

$$\begin{aligned} \lambda = \frac{\delta\mathcal{U}(ik + \hat{\kappa}K^2)[l^2 - k^2(1 + ik + \hat{\nu}K^2)]}{(\epsilon_s + ik + \hat{\kappa}K^2)} \\ \cdot \left\{\left(2 + ik + \hat{\nu}K^2\right)l^2 + \left(1 + ik + \hat{\nu}K^2\right) \right. \\ \left. \times \left[ik\left(3 + ik + \hat{\nu}K^2\right)\mathcal{U}^2 + k^2\right]\right\}^{-1}, \end{aligned} \tag{A4}$$

where $\hat{\nu} = \nu/\mathcal{U}$ and $\hat{\kappa} = \kappa/\mathcal{U}$. There are two types of instability present in the erosional mode, both of which are most easily detected by passing to the limit with $\nu \to 0$ and $\kappa \to 0$:

$$\lambda = \frac{ik\delta\mathcal{U}[l^2 - k^2(1 + ik)]}{(\epsilon_s + ik)\{(2 + ik)l^2 + k^2\left(1 - 4\mathcal{U}^2\right) + ik\left[3\mathcal{U}^2 + k^2\left(1 - \mathcal{U}^2\right)\right]\}}. \tag{A5}$$

First, consider modes with short transverse wavelength, i.e., $l \gg 1$:

$$\lambda \approx \frac{\delta\mathcal{U}[2k^2 + \epsilon_s k^2 + ik(2\epsilon_s - k^2)}{(4 + k^2)(\epsilon_s + k^2)}. \tag{A6}$$

Sufficiently short transverse waves are therefore always unstable, independently of the strength of the flow (although the growth rate remains proportional to the flow speed). These instabilities are the analogues of the landscaping modes of *Smith and Bretherton* [1971] and would evolve into channels aligned downhill (i.e., they are channelization instabilities).

[38] Next consider modes with very long transverse scale: $l \to 0$. In this case,

$$Re(\lambda) = \frac{k^2\delta\mathcal{U}\left[k^2\left(\mathcal{U}^2 - 1\right) - 3\mathcal{U}^2\epsilon_s\right]}{\left(\epsilon_s^2 + k^2\right)\left[9\mathcal{U}^4 + k^2\left(1 - \mathcal{U}^2\right)^2\right]}. \tag{A7}$$

Slow flows are therefore stable to this type of incisional modes, but sufficiently fast flows are unstable. The unstable modes are the cyclic steps of *Parker and Izumi* [2000], and migrate upstream like the bed forms seen in experiments (Figure 5).

[39] Note that, for all l, one can analytically deduce the $(\nu = \kappa = 0)$ stability boundary on the (k, l)-plane. For $\epsilon_s = 0$, for example, this is

$$\begin{aligned} l^2 = \frac{1}{4}k^2 \\ \times \left[1 + 4\mathcal{U}^2 + k^2 \pm \sqrt{\left(1 + 4\mathcal{U}^2 + k^2\right)^2 + 8\left(1 - \mathcal{U}^2\right)(1 + k^2)}\right], \end{aligned} \tag{A8}$$

which is pictured for various parameter settings in Figure A1.

[40] For all the types of instability, the role of ν is to stabilize short-waves ($K \gg 1$), but the longer-wave behavior remains relatively unaffected. This is illustrated in Figure A1, which also shows scaled growth rates, $Re(\lambda)/(\delta\mathcal{U})$, as a density over the (k, l)-plane for four choices of $\mathcal{U}$ and ν, with $\epsilon_s = 0$. The picture is much the same when $\epsilon_s \neq 0$, although, as expected from (A7), a finite streamwise wave number, k, is required for the cyclic step instability, and there are minor variations at smaller wave numbers (see the final panels of the figure).

[41] The channelization instability is clearly present for smaller $\mathcal{U}$, and ν reduces the growth rates at large l (although it does not cut off the instability). For $\mathcal{U} > 1$, the step instability enters strongly; again ν limits the wave numbers of the most unstable modes. For the parameters plotted, the

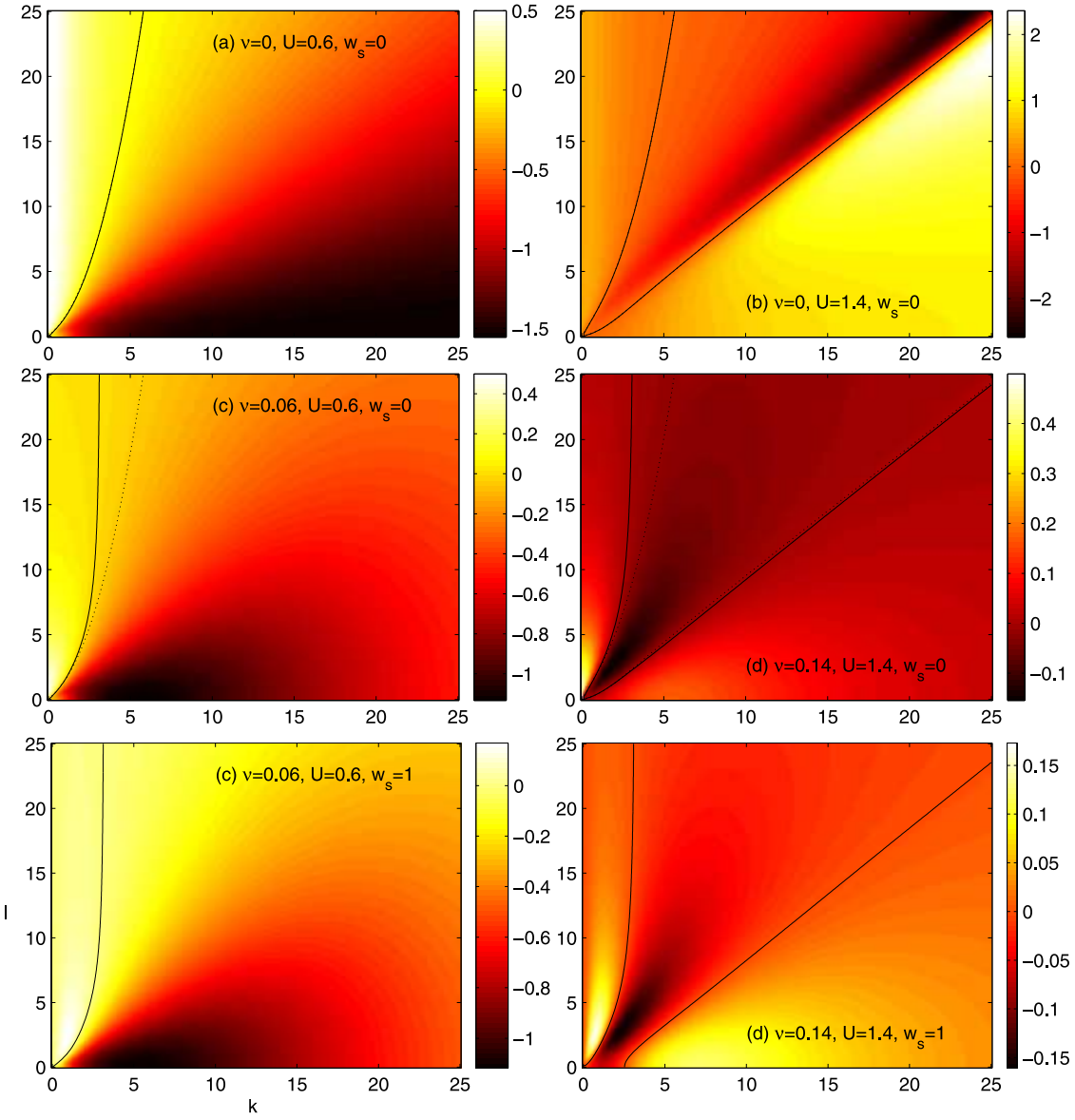

Figure A1. Scaled growth rates as densities over the (k, l)-plane for (a) $\nu = 0$ and $\mathcal{U} = 0.6$, (b) $\nu = 0$ and $\mathcal{U} = 1.4$, (c) $\nu = 0.06$ and $\mathcal{U} = 0.6$, and (d) $\nu = 0.14$ and $\mathcal{U} = 1.4$. $\epsilon_s = 0$. The dark, solid lines show the stability boundaries; the dotted lines show the $\nu = 0$ approximation of them (as given by (ss); in (a) and (b), the solid and dotted lines coincide). Panels (e) and (f) repeat (c) and (d), but with $\epsilon_s = 1$.

two types of instability remain distinct, and the step instability is the more dominant. The strongest instabilities emerge for rays with $k \sim l$: For $k \gg 1$ with $k \sim l$, we observe that

$$\lambda \sim \frac{\delta\mathcal{U}[k^2 + O(k)]}{\left[k^2\left(\mathcal{U}^2 - 1\right) - l^2 + O(k)\right]}, \tag{A9}$$

implying growth rates can potentially become large near the ray $l = k\sqrt{\mathcal{U}^2 - 1}$, which also is close to the stability boundary. A finer analysis indicates that the growth actually saturates for large k, and it flattens out to a maximum at the shortest waves (which is somewhat unphysical, though not mathematically ill-posed).

[42] **Acknowledgments.** The experiments were performed at the Geophysical Fluid Dynamics Summer Program, Woods Hole Oceanographic Institution, and we enjoyed numerous demonstrations to the crowds on the porch of Walsh Cottage. We thank Claudia Cenedese, Karl Helfrich and Jack Whitehead for allowing us to make a mess in the Coastal Research Laboratory, and Keith Bradley for technical assistance.

References

Arakawa, A., and V. Lamb (1977), Computational design of the basic dynamical processes of the UCLA general circulation model, *Methods of Computational Physics 17* (Academic Press, New York), 174–267.

Balmforth, N. J., and A. Provenzale (Eds.) (2001), *Geomorphological Fluid Mechanics*, Springer-Verlag, Berlin.

Blown, I. G., and M. Church (1985), Catastrophic lake drainage within the Homathko River Basin, British Columbia, *Can. Geotech. J.*, *22*, 551–563.

Boris, J. P., and D. L. Book (1976), Solution of Continuity Equations by the Method of Flux-Corrected Transport, in *Methods of Computational Physics 16* (Academic Press, New York), 85–129.

Cao, Z., G. Pender, S. Wallis, and P. Carling (2004), Computational dam-break hydraulics over erodible sediment bed, *J. Hydraul. Eng. ASCE*, *130*, 689–703.

Clague, J. J., and S. G. Evans (2000), A review of catastrophic drainage of moraine-dammed lakes in British Columbia, *Quat. Sci. Rev.*, *19*, 1763–1783.

Coleman, S. E., D. P. Andrews, and M. G. Webby (2002), Overtopping breaching of noncohesive homogeneous embarkments, *J. Hydraul. Eng. ASCE*, *128*, 829–838.

Costa, J. E., and R. L. Schuster (1988), The formation and failure of natural dams, *Bull. Geol. Soc. Am.*, *100*(7), 1054–1068.

Froehlich, D. C. (1995), Peak outflow from breached embankment dam, *J. Water Resour. Plan. Manage. Div., ASCE*, *121*(1), 90–97.

Hubbard, B., A. Heald, J. M. Reynolds, D. Quincey, D. S. Richardson, M. Zapata Luyo, N. Santillan Portilla, and M. J. Hambrey (2005), Impact of a rock avalanche on a moraine-dammed proglacial lake: Laguna Safuna Alta, Cordillera Blanca, Peru, *Earth Surf. Processes Landforms*, *30*, 1251–1264.

Jeffreys, H. (1925), The flow of water in an inclined channel of rectangular bottom, *Philos. Mag.*, *49*, 793–807.

Kershaw, J. A., J. J. Clague, and S. G. Evans (2005), Geomorphic and sedimentological signature of a two-phase outburst flood from moraine-dammed Queen Bess Lake, British Columbia, Canada, *Earth Surf. Processes Landforms*, *30*, 1–25.

McDonald, T. C., and J. Langridge-Monopolis (1984), Breaching characteristics of dam failures, *J. Hydr. Eng. ASCE*, *110*(5), 567–586.

Parker, G., and N. Izumi (2000), Purely erosional cyclic and solitary steps created by flow over a cohesive bed, *J. Fluid Mech.*, *419*, 203–238.

Parker, G. (2006), *1D sediment transport morphodynamics with applications to rivers and turbidity currents*, last updated April 13 2006. http://cee.uiuc.edu/people/parkerg/morphodynamics_e-book.htm

Seminara, G. (2001), Invitation to Sediment Transport, in *Geomorphological Fluid Mechanics*, N. J. Balmforth and A. Provenzale (Eds.), Springer-Verlag, Berlin.

Singh, V. P. (1996), *Dam breach modeling technology.*, Kluwer Academic Publisher, Dordrecht.

Singh, V. P., and P. D. Scarlators (1988), Analysis of gradual earth-dam failure, *J. Hydraul. Eng. ASCE*, *114*(1), 21–42.

Smith, T. R., and F. P. Bretherton (1971), Stability and the conservation of mass in drainage basin evolution, *Water Resour. Res.*, *8*, 1506–1529.

Tingsanchali, T., and C. Chinnarasri (2001), Numerical model of dam failure due to flow overtopping, *Hydrol. Sci. J.*, *46*(1), 113–130.

Walder, J. S., and J. E. O'Connor (1997), Methods for predicting peak discharge of floods caused by failure of natural and constructed earthen dams, *Water Resour. Res.*, *33*(10), 2337–2348.

Wang, Z., and D. S. Bowles (2006a), Three-dimensional non-cohesive earthen dam breach model. Part 1: Theory and methodology, *Adv. Water Resour.*, *29*, 1528–1545.

Wang, Z., and D. S. Bowles (2006b), Three-dimensional non-cohesive earthen dam breach model. Part 2: Validation and applications, *Adv. Water Resour.*, *29*, 1490–1503.

Wurbs, R. A. (1987), Dam-breach flood wave models, *J. Hydraul. Eng. ASCE*, *113*(1), 29–46.

Zalesak, S. T. (1979), Fully multidimensional flux-corrected transport, *J. Comput. Phys.*, *31*, 335–362.

Zammett, R. (2006), Breaking moraine dams by catastrophic erosional incision, *Proceedings, Geophysical Fluid Dynamics Summer Study Program*, Woods Hole Oceanographic Institution, Technical Report WHOI-2007-02. http://www.whoi.edu/cms/files/Rachel_21238.pdf

Zech, X. X., and X. X. Spinewine (2002), Dam-break induced floods and sediment movement - state of the art and need for research, First Workshop of the EU Project IMPACT, HR Wallingford, http://www.gce.ucl.ac.be/hydraulique/recherches/recherches/rechbs/publis/pap02Wal1-screen.pdf

N. J. Balmforth, Departments of Earth and Ocean Science and Mathematics, University of British Columbia, Vancouver, BC, Canada. (njb@math.ubc.ca)

A. Provenzale and J. von Hardenberg, Institute of Atmospheric Sciences and Climate, CNR, Corso Fiume 4, 10133 Torino, Italy. (a.provenzale@isac.cnr.it; j.vonhardenberg@isac.cnr.it)

R. Zammett, Department of Mathematics, University of Oxford, UK. (rachel_zammett@yahoo.co.uk)